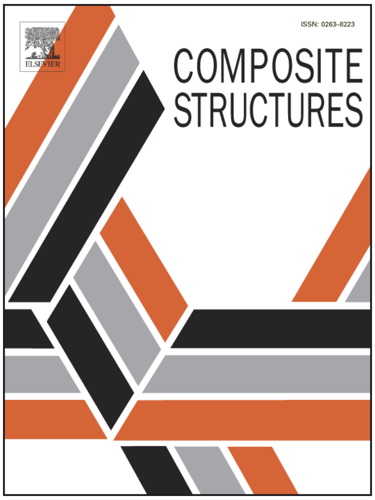

Experimental and numerical investigation of the impact response of elastomer layered fiber metal laminates (EFMLs)

Alireza Taherzadeh-Fard, Gholamhossein Liaghat, Hamed Ahmadi, Omid Razmkhah, Sahand Chitsaz Charandabi, Mohammad Amin Zarezadeh-mehrizi, Amin Khodadadi

PII: S0263-8223(19)34112-1
DOI: https://doi.org/10.1016/j.compstruct.2020.112264
Reference: COST 112264

To appear in: *Composite Structures*

Received Date: 28 October 2019
Accepted Date: 23 March 2020

Please cite this article as: Taherzadeh-Fard, A., Liaghat, G., Ahmadi, H., Razmkhah, O., Chitsaz Charandabi, S., Amin Zarezadeh-mehrizi, M., Khodadadi, A., Experimental and numerical investigation of the impact response of elastomer layered fiber metal laminates (EFMLs), *Composite Structures* (2020), doi: https://doi.org/10.1016/j.compstruct.2020.112264

Experimental and numerical investigation of the impact response of elastomer layered fiber metal laminates (EFMLs)

Alireza Taherzadeh-Fard [a], Gholamhossein Liaghat[a, b,]*, Hamed Ahmadi [a], Omid Razmkhah[c], Sahand Chitsaz Charandabi[c], Mohammad Amin Zarezadeh-mehrizi[a], Amin Khodadadi[a]

[a] Mechanical Engineering Department, TarbiatModares University, Tehran, Iran
[b] School of Mechanical & Aerospace Engineering, Kingston University, London, England, United Kingdom
[c] School of Mechanical Engineering, Coventry University, Coventry, United Kingdom

Abstract

The aim of the present study is to investigate the effect of introducing an elastomer layer into conventional fiber metal laminates on their perforation resistance. Natural compounded rubber as elastomeric media and glass/epoxy composite were sandwiched in between two layers of aluminum 6061-T6 and then the resulted structure was perforated by a 10 mm diameter hemispherical projectile at different impact velocities. Residual velocities were recorded by a high speed camera via a shadowing technique. Results showed that an elastomer layer located nearer to frontal face had a better energy absorbing performance due to load spreading; besides, by increasing the impact velocity the elastomer performs more efficiently because of the elastomer damage initiation point movement toward the periphery of the stretched area. Numerical simulation of penetration process was accomplished using the advanced finite element code of LS-DYNA. Finally, a numerical parametric study was performed to assess the effect of elastomer thickness on the energy absorption efficiency (EAE) of the whole structure. Based on the obtained results, adding an elastomeric layer into the structure is more beneficial than composite thickening at the same thickness in terms of improving EAE and reducing areal density.

Keywords: Fiber metal laminate; Elastomer; Impact resistance; Numerical simulation

---

*Corresponding author:Mechanical Engineering Department, TarbiatModares University,P.O. Box 14115-111, Tehran, Iran. E-mail address: ghlia530@modares.ac.ir, Tel. +98-2182883387

1. Introduction

In recent years, innovation and application of composite materials has been considered as a landmark in modern industrial design. Due to some features such as high ductility, low weight and excellent structural stability, these materials has attracted much attention [1]. Accordingly, many attempts have been dedicated to improve the penetration resistance of composites in related research area. Due to works conducted so far, application of one or more layers of a hard material along with the fiber composite layers can reduce the impact induced damage and impact sensitivity of the resulted structure [2, 3]. Fiber Metal Laminates (FMLs) which are composed of alternating metallic and composite layers are one of the most popular of such structures and their high velocity impact response has been argued comprehensively [4-6]. This laminate has been of interest due to have a blend of metallic properties including isotropy, durability, plastic behavior, impact resistance and ease of repairing and composite properties such as high strength, stiffness and fatigue resistance [7].

Due to ductile nature of the aluminum, impact load is not a threat for this phase since it could bear high amount of deformation in elastic region; However, composite layers are brittle in nature which accounts for low energy absorbing in elastic region before undergoing different failure modes [7]. One solution to this problem would be using elastomer rather than or beside the composite phase. Mohotti et al. [8] investigated the different configurations of aluminum/polyurea composite plate under high velocity impact in terms of reduction of the residual velocity, damage mechanism and kinetic energy absorption of the plates. They concluded that a thick plyurea coating on the back side of composite plates could contribute positively in reduction of residual velocity. Later they also assessed the behavior of this laminate analytically and numerically [9].

Sarlin et al. [2] investigated the performance of steel/rubber/composite plates and concluded that the rubber could decrease the damage area by an amount of 50%. This damage area was observed to increase proportionally by the impact energy. Xue et al. [3] studied the steel/polyurea laminates at sub-ordnance range impact velocities. They showed that not only does elastomer contribute to the impact resistance improvement by storing energy within the elastomeric media but it also increases the energy absorption capacity of steel layer. Bogoslovov et al. [10] investigated the steel/elastomer bilayers under high velocity impact and reported that for elastomers with relatively high glass transition temperature, if the impact induced strain rate lies in the range of segmental dynamics frequency, a transition from rubbery to glassy state can be occurred which leads to high amount of energy dissipation. Roland et al. [11] further discussed about the parameters influences this viscoelastic phase transition and asserted that the elastomer coated steel laminate could be more effective when using a harder and thinner substrate. Grujicic et al. [12] have simulated this behavior numerically. Khodadadi et al. [13] investigated the perforation behavior of hyper elastic rubber panels and concluded that the higher amount of elastomer hardness could lead to its better perforation resistance.

In addition to expected improvement in perforation resistance, adding elastomer to structure could tackle some other shortcomings. Stoll et al. [14] have asserted that applying an elastomer interlayer in carbon fiber reinforced aluminum laminates could reduce the coefficient of thermal expansion mismatch and galvanic corrosion. Stoll and Weidenmann[15] have investigated fatigue properties of FMLs containing an elastomer interlayer and reported superior improvement in endurance limit; besides, Sessner et al. [16] evaluated the damping properties of such laminate and reported the positive influence of a soft elastomer in improving the damping capacity. Liebig et al. [17] and Stoll et al. [18] investigated the factors influencing damping and mechanical properties of this laminate experimentally and numerically and observed a dependency of natural frequencies in various modes and flexural stiffness on elastomer thickness.

At the present study, high velocity perforation behavior of laminates consists of aluminum as outer layers and glass fiber reinforced polymer and compounded natural rubber as core materials is investigated. This arrangement can be considered as a mutated version of typical fiber metal laminates which includes a layer of elastomer (EFML[1]). The purpose of studying such a structure is to maintain the stiffness as well as to increase the energy absorption capacity which has not been assessed in previous studies. Specimens were assessed in terms of damage mechanisms and impact resistance. The commercially available 3D dynamic nonlinear software, LS-DYNA, was used to simulate the dynamic behavior of the specimens. A numerical parametric study was accomplished to investigate the effect of elastomer and composite thicknesses on perforation efficiency.

2. Experimental Procedure

2.1. Materials

The laminated composites consist of three discrete phase of materials. The outer layers are aluminum 6061-T6 obtained from AMAG rolling GmbH with a thickness of 0.5 mm. The composite layer includes plain-weave glass fiber, 200 gr/m^2 in areal weight, and ML-506 epoxy resin. They were purchased from Metyx company, Turkey

---

[1] Elastomer layered Fiber Metal Laminate

and Mokarrar indutrial group, Iran, respectively. The elastomer is a kind of natural rubber (SMR 20) with Mooney viscosity of 65 which is supplied by the Rubber Research Institute of Malaysia. Natural rubber was preferred to other types of elastomer because of its superior damping capacity, tear resistance and flexibility [19]. To improve the mechanical properties, some ingredients as carbon black and calcium carbonate were added to the compound [20]; besides, ZnO, stearic acid, accelerators and sulfur, obtained from LG, Korea, were used to construct vulcanization bonding process. The final mass density of the elastomer was measured as 1255 kg/m^3. An elaborated description of ingredient loadings is listed in Table 1.

Table 1

Two different adhesives were used to bond the layers [21]. For elastomer/aluminum interface the Chemosil 222 and its primer (Chemosil 211) obtained from LORD corporation were applied. In elastomer/composite and composite/aluminum interface the Bylamet-S2 adhesive (BYLA GmbH) was used which is a one component cyanoacrylate adhesive based on modified ethylenester and is excellent for bonding plastics, rubbers and metals.

2.2. Sample preparation

The first stage in fabrication process is to accomplish the binding between elastomer and aluminum layers. To do so, the surface preparation of aluminum according to ASTM standard D2651 was conducted and thin layers of Chemosil adhesive and its primer were brushed onto its surface. Thereafter, the coated aluminum layer and un-vulcanized rubber were placed for 4 minutes at a 25-ton hydraulic hot press (Davenport, England) at a temperature of 160 ºC to complete the interface bonding and vulcanizing the rubber simultaneously. The vulcanizing conditions of the compounded rubber had been obtained during a rheometer test. Since then, a six-layer glass/epoxy composite as well as an aluminum layer were attached to the elastomer/aluminum bi-layer at room temperature. Some FML samples were also fabricated for comparison purposes. Fig. 1 shows the final specimen arrangement schematically. The thickness of aluminum, elastomer and composite was 0.5, 2.62 and 1.91 mm respectively. The nominal in plane dimensions of the laminates were 120×120 square millimeters.

Fig. 1

2.3. Characterization

To obtain the material properties of the GFRP[2], three kind of tests i.e. tensile, shear and compression were performed according to ASTM standards D3039, D3518 and D 3410, respectively. DIC[3] method was used to strain detecting during the tests. The obtained properties of the GFRP is presented in Table 2.

Table 2

Split Hopkinson Pressure Bar (SHPB) was employed to obtain stress-strain curves of the elastomer at different strain rates. To minimize the effects of inertia and friction, optimum value of 0.5 was chosen for specimens length to diameter ratio [22]; besides, a length of 5mm was chosen for elastomeric coupons to ensure a uniform deformation and stress equilibrium during the test. Stress-strain curves of the elastomer are represented in Fig. 2 through different strain rates.

Fig. 2

---

[2] Glass Fiber Reinforced Polymer

[3] Digital Image Correlation

2.4. Test Procedure

High velocity impact tests were carried out using a gas gun apparatus in which compressed air controlled by a solenoid valve was used to accelerate the projectile through a 6m long barrel. Impact velocity of the projectile was measured by means of two laser gauges just before collision with the target; in addition, the residual velocity was obtained using a high speed camera (PhotronFastcam Super 10KC, Tokyo, Japan) via a shadowing technique as presented in Fig. 3. In this method, a uniformly distributed light source is located directly in front of the high speed camera with a right angle and the shadow of the projectile passing in between is recorded at certain time intervals.

Fig. 3

All specimens were fully clamped in a fixture having a 100×100 square millimeters opening. The projectile was made of steel with a hemispherical nose shape which weighed 9.33 grams and had been hardened to 53 Rockwell C; therefore, it can be considered as rigid and non-deformable. Technical information of the fixture and projectile is presented in Fig. 4.

Fig. 4

To assess the influence of the elastomer interlayer on perforation behavior of laminates, the samples were tested in two methods in which the elastomer was located either at the impacted side (Elastomer Forward or EF) or back side (Elastomer Backward or EB) of the laminate. A laminate without elastomer (WE) was also considered as a reference for comparison purposes. An illustration of different sample arrangements is given in Table 3. All specimens were tested at two different impact velocities of 166 and 196 m/s.

Table 3

3. Numerical Simulation

3.1. Geometry Modeling

The simulations were accomplished by means of the commercial finite element code LS-DYNA in double precision mode. To reduce the computational time, only a quarter of the structure was considered and symmetric boundary conditions were applied to eliminate the effect of this size reduction; besides, eight-node solid elements with reduced integration point formulation were chosen to describe the state of stress. A biased mesh for in plane dimensions was adopted in which a fine mesh in impacted area is becoming coarse toward the edges of the plies. In order to consider the transverse wave propagation in different plies, at least two elements were considered for each ply in through the thickness direction. To achieve a realistic boundary conditions, the clamp was also included in modeling rather than simply constraining the boundary nodes. A mesh study was conducted so that the minimum element size was reduced from 0.5 to 0.15 mm during which a mesh independency was observed at the minimum element size of 0.21 mm. The total number of elements of a composite ply, elastomer and a layer of aluminum was measured to be 20000, 130000 and 20000 respectively. A detailed view of the finite element model is presented in Fig. 5.

Fig. 5

3.2. Material Models

3.2.1. Aluminum

One of the most functional models to describe the visco-plastic behavior of materials under a wide range of strain rates is Johnson-Cook which has been used in numerous researches [23-25]. The benefit of this material model over some other formulations such as Cowper-Symonds is the consideration of strain hardening as well as temperature effects and is known as *MAT_JOHNSON_COOK (MAT_15) in LS-DYNA. The formulation of this material model is as below:

$$\sigma_y = (A + B\bar{\varepsilon}^{p^n})(1 + c\, ln\dot{\varepsilon}^*)(1 - T^{*^m}) \tag{1}$$

where σ_y and A are flow and yield stresses, B and n are strain hardening parameters, c is the strain rate effect parameter and m is thermal softening exponent; Besides:

$\bar{\varepsilon}^p =$ effective plastic strain

$\dot{\varepsilon}^* = \frac{\dot{\bar{\varepsilon}}^p}{\dot{\varepsilon}_0} =$ dimensionless plastic strain rate and

$$T^* = \frac{T - T_{room}}{T_{melt} - T_{room}} \tag{2}$$

where T_{room} and T_{melt} areroom temperature and melting point in absolute scale, respectively.

This material model also uses a linear accumulating formulation to calculate the failure strain as:

$$\varepsilon^f = [D_1 + D_2\, exp\, D_3\sigma^*][1 + D_4 \ln \varepsilon^*][1 + D_5T^*] \tag{3}$$

where σ^* is the ratio of the mean stress to the effective stress and $D_1 - D_5$ are failure parameters which can be obtained experimentally. Damage in aluminum will occur when the damage parameter (D) reaches unity:

$$D = \sum \frac{\Delta \bar{\varepsilon}^p}{\varepsilon^f} \tag{4}$$

The required parameters for aluminum 6061-T6 are obtained from open literature and presented in Table 4.

Table 4

3.2.2. Glass/epoxy composite

To describe the behavior of laminated composites, LS-DYNA introduces a variety of material models of which *MAT_COMPOSITE_FAILURE (MAT_59) has been used in this study. MAT_59 is an orthotropic material model which not only does require less experimental data but it also is capable of considering the progressive damage of the material by means of a 3-dimensional stress based failure criterion. The onset of damage is occurred on the basis of the following four independent criteria [27, 28]:

- Longitudinal and transverse tensile failure,
- Through the thickness shear failure,
- Longitudinal and transverse compressive failure, and
- Through the thickness compressive failure.

As example, longitudinal tensile failure occurs when the following relation is fulfilled:

$$\left(\frac{\sigma_1}{S_1}\right)^2+\left(\frac{\sigma_{12}}{S_{12}}\right)^2+\left(\frac{\sigma_{13}}{S_{13}}\right)^2\geq 1 \qquad (5)$$

where S and σ are strengths and developed stresses during deformation. When the criterion is satisfied, the corresponding modulus i.e. E_1 declines to zero and the load carrying capacity in longitudinal direction is eliminated. Other criteria's formulation is similar as that mentioned in Eq. (5). It is worth to mention that the failure criteria act independently and the satisfaction of one does not affect the performance of the others.

In order to prevent some instabilities, MAT_ADD_EROSION was attached to composite material model for element deletion after element failure based on a reasonable strain limit criterion.

3.2.2.1. strain rate effect

The material models available for composites in LS-DYNA software are not able to consider the strain rate effects completely. To include this effect in presented numerical simulation, it is reasonable to change the moduli and strengths due to high rate deformations according to the research conducted in this area. This method has been used in related researches to simulate impact response of GFRPs [28, 29]. A summary of property changes of the GFRP which has been used in this research is presented in Table 5.

Table 5

3.2.3. elastomer

A two parameter Mooney-Rivlin model was chosen to simulate the rubbery behavior of elastomer which is available in LS-DYNA as:

- *MAT_MOONEY-RIVLIN_RUBBER (MAT_27)

Benefiting from a strain energy density function as follows:

$$W = A(I - 3) + B(II - 3) \tag{6}$$

in which $2(A + B)$ is shear modulus of linear elasticity. Moreover, I and II are invariants of the right Cauchy-Green deformation tensor. A and B are fitting parameters and should be determined empirically. As the elastomer is considered incompressible, third invariant of right Cauchy-Green deformation tensor will equal unity.

As it was observed in Fig. 2, the elastomer is highly strain rate dependent while the material model is unable to include this effect. Nonetheless, the Mooney-Rivlin model can be employed with certain adjustment as mentioned in ref [36]. A number of primary simulations revealed that the order of strain rate was 10^3; therefore, curve fitting on the stress-strain diagram at the strain rate of 4000/s by least square method led to amounts of 5.6 MPa and 0.5 MPa for A and B, respectively. A maximum principal strain criteria was used for element erosion.

3.3. delamination modeling and contact definition

CONTACT_AUTOMATIC_SURFACE_TO_SURFACE_TIEBREAK was chosen in aluminum/composite and aluminum/elastomer interfaces. In this algorithm, the nodes which are initially in contact are tied together until a specified criterion is met as below:

$$\left(\frac{|\sigma_n|}{NFLS}\right)^2 + \left(\frac{|\sigma_s|}{SFLS}\right)^2 \geq 1 \qquad (7)$$

where σ_n and σ_s are current developed normal and shear stresses while NFLS and SFLS are interfacial normal and shear strengths, respectively. By satisfaction of equation 13, the interfacial nodal stresses are reduced to zero and the two engaged nodes are released. In this study, according to the adhesive manufacturer's datasheet, the interlaminar shear and normal strengths for aluminum/composite interface were chosen to be 19 MPa and 17 MPa, respectively. For elastomer/aluminum interface a value of 130 MPa was selected for interfacial strength during a trial and error procedure. As it can be observed in Fig. 6 which shows a specimen cross section after impact, there was not any clear separation of elastomer and composite layers; hence, CONTACT_TIED_SURFACE_TO_SURFACE was selected for this interface. The similar contact definition was also considered in ref. [9].

Fig. 6

Interaction between projectile and the whole structure was defined by CONTACT_ERODING_SURFACE_TO_SURFACE with segment based formulation [37].

4. Results and discussion

The considered configurations were perforated at impact velocities of 166 and 196 m/s. Comprehensive discussions are presented in subsequent sections of this paper. Note that each sample configuration and its test condition is designated by a code. For example, EF-166 represents the Elastomer forward configuration tested at the impact velocity of 166 m/s.

4.1. failure mechanisms and damage assessment

In order to design resistive structures against perforation, it is vital to have an elaborate understanding of the failure mechanisms. Front and back faces of the perforated specimens are presented in Fig. 7.

Fig. 7

During perforation process, it is difficult to identify a unique failure mechanism; however, multiple mechanisms as well as structural deformations contribute to the structure behavior. Considering the front faces in Fig. 7, it is apparent that a shear plugging mode in aluminum layer has occurred in almost all specimens. In early stages of the perforation process, high velocity contact with frontal aluminum layer can cause developing some severe transverse shear stresses which in turn could lead to some circumferential cracks around the impacted zone. These cracks and stresses are responsible for the plug sheared from the aluminum face. During this shearing process, some localized out of plane bending deformations are also occurred which cause developing circumferential tensile stresses that are in charge of the radial cracks near the impacted zone. This process is similar to the ductile crater enlargement mode which occurs in intermediate to thick targets [8].

Observing the back faces, it is apparent that the dominant mode is petaling which is produced by high radial and circumferential tensile stresses after passage of the initial wave occurring near the lip of the projectile [38]. This out of plane deformation is the result of bending moments created by forward motion of the projectile.

Another observation from the back faces can be the composite failure mode. Referring to Fig. 8, in WE specimens the dominant failure mechanism is shear plugging; however, it has been changed to fiber tensile failure in EF samples as can be seen as some star-shaped cracks propagated in the composite phase. This phenomenon could be justified according to the placement of an elastomeric layer next to the GFRP composite in EF samples. Indeed, high capability of elastomer to stretch prior to failure can distribute the exerted load and engage a wider area of the composite in the deformation process which leads to development of some tensile rather than shear stresses in this layer.

Fig. 8

At the considered impact velocities, the elastomer layer tears in a piercing mode in which some radial cross-shaped cracks are developed near the impacted area. As can be seen in Fig. 7, the crater diameter in elastomer layer is smaller than the other layers; this is due to the high capability of large elastic strains recovery in elastomer layer and contributes positively to velocity reduction [8]; besides, as it is shown in Fig. 9, in all EF specimens a bi-layer plug of elastomer and aluminum was sheared off which is an indication of localized loading and has also been observed by Xue et al. [3]. In WE and EB samples, single-layer aluminum plug and composite debris were observed to be ejected from the plate during perforation.

Fig. 9

To assess through the thickness failures and delamination, the cross section of the specimens was obtained by a water jet process and is presented in Fig. 10.

Fig. 10

At the beginning of the penetration process, some compressive waves are propagated through the target in the same direction as the projectile movement. Arriving at the interfaces, where the material is changed, some portion of this impact wave is transmitted as a compressive wave to the next layer and the other portion is reflected to the same media as a tensile wave. The reflected portion can cause developing of some intra-lamina cracks or inter-lamina failures (delamination). As illustrated in Fig. 10, in almost all samples, there is a severe debonding between aluminum and composite; in addition to the stiffness differences and adhesive performance, this separation could be attributed to the reflected tensile waves and the poor damping capacity of the engaged layers. As another observation, while there are some delaminations in composite laminate near the impacted area, there is not any debonding between elastomer and composite layers as mentioned before which can be justified according to the wave damping capacity and considerable flexibility of the elastomer. This has also led to a smaller debonding between elastomer and aluminum layers especially in the EF samples.

It is also important to assess if the numerical model is able to predict the failure mechanisms precisely; therefore, the post-mortem experimental and numerical configurations of EF-166 and WE-166 specimens are comprised in Fig. 11 as examples.

Fig. 11

It is evident that the failure mechanisms resulted from numerical modeling are similar to their experimental counterparts; the elastomer/aluminum bi-layer plug in EF samples and also the one-layer aluminum plug in WE specimens are predicted numerically as shown in Fig. 11.

4.2. perforation performance

High velocity perforation results are presented in Table 6. As it can be seen, application of elastomer obviously reduces the residual velocity at both impact velocities; however, this reduction is more in the case of EF. The similar result was achieved by Roland et al. [11] which can be attributed to the ability of elastomer in spreading the impact load.

Table 6

As presented in Fig. 12, in the case of EF, by positioning of the elastomer near the front face, more layers engage in the deformation process which consequently leads to a local pressure reduction and exerting a more severe negative acceleration to the projectile; indeed, in EF samples in addition to the stretching, the elastomer is capable of spreading out the impact load on the composite layer. In EB samples, however, the only functional ability of the elastomer is expected to be the elastic stretching.

Fig. 12

According to Table 6, the numerical results are in a good agreement with experimental data and the finite element model is accurately predicting residual velocities. Velocity time history of the projectile at impact velocity of 166 m/s has been obtained from numerical model and presented in Fig. 13.

Fig. 13

In early stages of penetration (region A), none of the elastomer energy absorbing mechanisms (load spreading and elastic stretching) are active; hence, all three configurations have the same behavior. During region ‘B’, however, the EF specimen finds a superior performance. To describe more clearly, perforation time sequences of EF-166 is presented in Fig. 14. The role of elastomer in engaging areas far from collision is started at t=0.05 ms and is maximized at t=0.2 ms just before the elastomer tearing. At this moment, the deflection of the whole laminate is seen to be maximized. At time t=0.23 ms the elastomer is torn and the projectile reaches its residual velocity.

Fig. 14

In order to maintain the consistency in comprising different configurations, it is necessary to eliminate mass dependency of measured quantities; Because the high velocity perforation is inherently localized, it is better to consider the areal density rather than mass which is defined as below:

$$d = \sum h_i \times \rho_i \tag{8}$$

In which h_i and ρ_i are the thickness and mass density of the layers. The areal densities of the specimens have been calculated to be 8.82 and 5.53 kg/m^2 for elastomer containing (EF and EB) and without elastomer (WE) samples, respectively. To compare the perforation performance, Energy Absorption Efficiency (EAE) is defined as:

$$EAE = \frac{\frac{1}{2}M\left(v_i^2 - v_r^2\right)}{\frac{1}{2}M v_i^2 d} = \frac{v_i^2 - v_r^2}{v_i^2 d} \tag{9}$$

where M, v_i and v_r are projectile mass, impact and residual velocities, respectively. The energy absorption efficiency is calculated for the specimens and presented in Fig. 15.

Fig. 15

As it can be seen, by increasing the impact velocity, the efficiency of the laminate decreases in all configurations. This has also been observed by Wang et al. [39] in Carbon/epoxy composites and by VanderKlok et al. [40] in glass/epoxy systems and is attributed to existing a critical velocity, at velocities above which a localization is occurred. When the impact velocity varies from below to above critical velocity, the failure modes are switched from global deformations and tensile damages to local shear failures. It is expected here that the critical velocity lies below or in the range of 166 to 196 m/s so that a reduction in performance with speed is observed.

Comprising the EAE of specimens at the impact velocity of 166 m/s, a reduction is observed with respect to WE in both EB and EF samples. This is an illustration of more energy absorption in elastomer containing samples at the cost of mass; however, EF has still a better performance than EB because of the load spreading function of elastomer in EF samples as described earlier. At the impact velocity of 196 m/s, while EB has approximately the same performance as WE, EF specimen performs better than WE and EB by an amount of 25 and 22 percent, respectively. Since the efficiency of the WE specimens had shown a declining trend by impact velocity, the reason should be searched in elastomer performance.

To assess the isolated elastomer performance, it can be assumed that the layers contribution to velocity reduction is additive. This method has been used in numerous studies [8, 11] and is an acceptable way to quantify the elastomer role in perforation process. To begin with, the velocity reduction in WE specimen is subtracted from its elastomer-containing counterpart at the same impact velocity to give the elastomer contribution to velocity reduction; the result is divided by the areal density of the elastomer to give the velocity reduction per unit areal density of elastomer which is presented in Fig. 16.

Fig. 16

From the obtained results, it can be observed that by increasing the impact velocity, the elastomer performance is improved in both EB and EF samples. This phenomenon cannot have any relations with the position of the elastomer because of its occurrence in both cases but would be attributed to the failure mechanism of the elastomer. To describe, a scheme of the elastomer during the perforation process is represented in Fig. 17.

Fig. 17

In the case of relatively low impact velocities, the elastomer has more sufficient time to spread the exerted deformation by means of the propagated in-plane and transverse waves; therefore, this layer deforms uniformly and the damage initiation point will be located near point ‘A’ which is critical from the maximum strain point of view. Increasing the impact velocity, the elastomer does not have enough time to meet the compatibility with strain rate and thus the critical point moves toward the periphery portion of deformation profile i.e. point ‘B’. This transition leads to a larger area being engaged in the damage initiation region which in turn improves the resistance behavior. To support this claim, in addition to the high velocity tests, some quasi-static indentation tests were also conducted at a rate of 2 mm/min with the same indenter nose shape as the projectile used in high velocity tests. Discussion about the details of this test is out of scope of the present paper; however, the failure mode of elastomer during the indentation test is compared with a high velocity perforated (EB-196) specimen in Fig. 18.

Fig. 18

As illustrated, in quasi-static test, the crack initiation and development spot in elastomer is located exactly under the tip of the indenter and is propagated through a linear passage; however, in high velocity perforated specimen, a plug formation is observable which is an indication of critical damage point movement to the periphery of the stretched area at high rates of deformation.

4.3. parametric study

4.3.1. effect of elastomer thickness

It is clear that increasing the elastomer thickness will result a decreasing in residual velocity; however, it is important to investigate if there will be an enhancement with respect to weight. To assess this issue, the elastomer thickness has been changed step by step - every stage about 0.65 mm - in numerical model. EAE is calculated for each state and presented in Fig. 19.

Fig. 19

As clear, the performance of both elastomer containing samples are approximately constant in the considered range of elastomer thickness variations. This is an indication of equivalent changes in velocity reduction and mass mounting in a manner that no changes are observed in EAE. As the thickness further increases, bending moment required to deform the elastomer increases and effect of the other layers are less pronounced in a way that in very high amount of elastomer thickness, there will be no difference between EF and EB specimens. The evidence of this phenomenon is the slight increase in EAE for EB samples as can be seen in Fig. 19.

4.3.2. composite thickening vs. elastomer addition

Due to the lower mass density and higher stretching ability of elastomer than composite, it is worth to assess whether the thickening of the composite phase or introducing an elastomeric layer can be more lucrative.

To investigate, a WE specimen with a composite phase thickness of 3.8 mm is considered. According to the better performance of the elastomer near the front face, half thickness of the composite is replaced by an elastomeric layer near the front face (EF) in a way that that the total laminate thickness remains constant. The two resulted structures are perforated at impact velocities of 166 and 196 m/s and the results are presented in Fig. 20.

Fig. 20

As it can be seen, perforation efficiency of the structure has improved by incorporating elastomeric layer by an amount of 39 and 48 percent at impact velocities of 166 and 196 m/s, respectively. The result is obtained while the areal density is also reduced from 8.3 m^2/kg in WE sample to 7.9 m^2/kg in the elastomer-containing specimen. It should be noted that reducing the composite layer thickness will have an adverse impact on structure stiffness and should be done with caution.

5. Conclusions

In present study, impact behavior of an elastomer containing version of conventional fiber metal laminates composed of aluminum as outer faces, elastomer and glass fiber reinforced polymer as core layers was investigated experimentally using a gas gun and numerically by LS-DYNA code.

The main damage mechanisms were observed to be petaling and shear plugging in aluminum layers, tensile fiber failure and plugging at GFRP and piercing at elastomer layer; in addition, a severe debonding between aluminum and composite was diagnosed which was justified according to the reflected tensile waves from interfaces and the poor damping capacity of the engaged layers. From the perforation performance point of view, at all impact velocities, locating the elastomer layer close to the frontal face allowed it to engage the composite layer in deformation process more efficiently, whereby the resistance performance was enhanced in comparison with the case of placing it close to the back side. The change of composite damage mechanism from shear plug in without-elastomer samples to tensile fiber failure in elastomer-forward specimens was an evident of this claim. In addition, despite of where the elastomer layer was located, by increasing the impact velocity, resistance performance of this layer was enhanced which was justified according to the critical damage initiation point movement of the elastomer to periphery of stretched area by mounting the impact velocity.

According to numerical results, although it is clear that increasing elastomer thickness contributes positively to residual velocity reduction, elastomer thickening had a negligible effect on the energy absorption efficiency of the whole structure in the thickness range of 2 mm to 4.6 mm; besides, incorporation of an elastomeric layer near the front face rather than increasing the composite thickness was shown to be more efficient as for energy absorption efficiency improvement and weight reduction by an amount of 40 and 5 percent, respectively.

Acknowledgements

The authors are grateful to TarbiatModares University (TMU) for its financial support.

Declaration of competing interest

None.

References

[1] Mohotti D, Ngo T, Raman SN, Ali M, Mendis P. Plastic deformation of polyurea coated composite aluminium plates subjected to low velocity impact. Materials & Design (1980-2015). 2014;56:696-713.
[2] Sarlin E, Apostol M, Lindroos M, Kuokkala VT, Vuorinen J, Lepistö T, et al. Impact properties of novel corrosion resistant hybrid structures. Composite Structures. 2014;108:886-93.
[3] Xue L, Mock W, Belytschko T. Penetration of DH-36 steel plates with and without polyurea coating. Mechanics of Materials. 2010;42(11):981-1003.
[4] Morinière F, Alderliesten R, Benedictus R. Modelling of impact damage and dynamics in fibre-metal laminates–a review. International Journal of Impact Engineering. 2014;67:27-38.
[5] Sadighi M, Alderliesten RC, Benedictus R. Impact resistance of fiber-metal laminates: A review. International Journal of Impact Engineering. 2012;49:77-90.
[6] Ahmadi H, Liaghat G, Sabouri H, Bidkhouri E. Investigation on the high velocity impact properties of glass-reinforced fiber metal laminates. Journal of Composite Materials. 2013;47(13):1605-15.
[7] Chai GB, Manikandan P. Low velocity impact response of fibre-metal laminates – A review. Composite Structures. 2014;107:363-81.
[8] Mohotti D, Ngo T, Mendis P, Raman SN. Polyurea coated composite aluminium plates subjected to high velocity projectile impact. Materials & Design (1980-2015). 2013;52:1-16.
[9] Mohotti D, Ngo T, Raman SN, Mendis P. Analytical and numerical investigation of polyurea layered aluminium plates subjected to high velocity projectile impact. Materials & Design. 2015;82:1-17.
[10] Bogoslovov R, Roland C, Gamache R. Impact-induced glass transition in elastomeric coatings. Applied physics letters. 2007;90(22):221910.

[11] Roland C, Fragiadakis D, Gamache R, Casalini R. Factors influencing the ballistic impact resistance of elastomer-coated metal substrates. Philosophical Magazine. 2013;93(5):468-77.
[12] Grujicic M, Pandurangan B, He T, Cheeseman B, Yen C-F, Randow C. Computational investigation of impact energy absorption capability of polyurea coatings via deformation-induced glass transition. Materials Science and Engineering: A. 2010;527(29-30):7741-51.
[13] Khodadadi A, Liaghat G, Ahmadi H, Bahramian AR, Anani Y, Razmkhah O, et al. Numerical and experimental study of impact on hyperelastic rubber panels. Iranian Polymer Journal. 2019;28(2):113-22.
[14] Stoll M, Stemmer F, Ilinzeer S, Weidenmann KA. Optimization of corrosive properties of carbon fiber reinforced aluminum laminates due to integration of an elastomer interlayer. Key Engineering Materials: Trans Tech Publ; 2017. p. 287-93.
[15] Stoll MM, Weidenmann KA. Fatigue of fiber-metal-laminates with aluminum core, CFRP face sheets and elastomer interlayers (FMEL). International Journal of Fatigue. 2018;107:110-8.
[16] Sessner V, Stoll M, Feuvrier A, Weidenmann KA. Determination of the Damping Characteristics of Fiber-Metal-Elastomer Laminates Using Piezo-Indicated-Loss-Factor Experiments. Key Engineering Materials: Trans Tech Publ; 2017. p. 325-32.
[17] Liebig WV, Sessner V, Weidenmann KA, Kärger L. Numerical and experimental investigations of the damping behaviour of hybrid CFRP-elastomer-metal laminates. Composite Structures. 2018;202:1109-13.
[18] Stoll MM, Sessner V, Kramar M, Technau J, Weidenmann KA. The effect of an elastomer interlayer thickness variation on the mechanical properties of Fiber-Metal-Laminates. Composite Structures. 2019;219:90-6.
[19] Yang H, Yao X, Zheng Z, Gong L, Yuan L, Yuan Y, et al. Highly sensitive and stretchable graphene-silicone rubber composites for strain sensing. Composites Science and Technology. 2018;167:371-8.
[20] Khodadadi A, Liaghat G, Bahramian AR, Ahmadi H, Anani Y, Asemani S, et al. High velocity impact behavior of Kevlar/rubber and Kevlar/epoxy composites: A comparative study. Composite Structures. 2019;216:159-67.
[21] Zarezadeh mehrizi ma, Taherzadeh-Fard A, Liaghat g, Ahmadi H, Anani Y, Khodadadi A, et al. Experimental investigation on the inter-laminar strength in a hybrid elastomer modified fiber metal laminate under high and low velocity impact and quasi-static bending. Amirkabir Journal of Mechanical Engineering. 2019;52(10):181-90.
[22] Bai Y, Liu C, Huang G, Li W, Feng S. A hyper-viscoelastic constitutive model for polyurea under uniaxial compressive loading. Polymers. 2016;8(4):133.
[23] Zhu Q, Zhang C, Curiel-Sosa JL, Quoc Bui T, Xu X. Finite element simulation of damage in fiber metal laminates under high velocity impact by projectiles with different shapes. Composite Structures. 2019;214:73-82.
[24] Burley M, Campbell JE, Dean J, Clyne TW. Johnson-Cook parameter evaluation from ballistic impact data via iterative FEM modelling. International Journal of Impact Engineering. 2018;112:180-92.
[25] Wang JX, Zhou N. Experimental and numerical study of the ballistic performance of steel fibre-reinforced explosively welded targets impacted by a spherical fragment. Composites Part B: Engineering. 2015;75:65-72.
[26] Chocron S, Erice B, Anderson CE. A new plasticity and failure model for ballistic application. International Journal of Impact Engineering. 2011;38(8-9):755-64.
[27] Giannaros E, Kotzakolios A, Kostopoulos V, Campoli G. Hypervelocity impact response of CFRP laminates using smoothed particle hydrodynamics method: Implementation and validation. International Journal of Impact Engineering. 2019;123:56-69.

[28] Menna C, Asprone D, Caprino G, Lopresto V, Prota A. Numerical simulation of impact tests on GFRP composite laminates. International Journal of Impact Engineering. 2011;38(8-9):677-85.
[29] Hoo Fatt MS, Lin C, Revilock DM, Hopkins DA. Ballistic impact of GLARE™ fiber–metal laminates. Composite Structures. 2003;61(1):73-88.
[30] Naik NK, Yernamma P, Thoram NM, Gadipatri R, Kavala VR. High strain rate tensile behavior of woven fabric E-glass/epoxy composite. Polymer Testing. 2010;29(1):14-22.
[31] Shokrieh MM, Omidi MJ. Tension behavior of unidirectional glass/epoxy composites under different strain rates. Composite Structures. 2009;88(4):595-601.
[32] Gowtham H, Pothnis JR, Ravikumar G, Naik N. High strain rate in-plane shear behavior of composites. Polymer Testing. 2013;32(8):1334-41.
[33] Shokrieh MM, Omidi MJ. Investigation of strain rate effects on in-plane shear properties of glass/epoxy composites. Composite Structures. 2009;91(1):95-102.
[34] Gillespie Jr J, Gama B, Cichanowski C, Xiao J. Interlaminar shear strength of plain weave S2-glass/SC79 composites subjected to out-of-plane high strain rate compressive loadings. Composites Science and Technology. 2005;65(11-12):1891-908.
[35] Ravikumar G, Pothnis JR, Joshi M, Akella K, Kumar S, Naik N. Analytical and experimental studies on mechanical behavior of composites under high strain rate compressive loading. Materials & Design. 2013;44:246-55.
[36] Khodadadi A, Liaghat G, Ahmadi H, Bahramian AR, Razmkhah O. Impact response of Kevlar/rubber composite. Composites Science and Technology. 2019:107880.
[37] Sevkat E, Liaw B, Delale F, Raju BB. Drop-weight impact of plain-woven hybrid glass–graphite/toughened epoxy composites. Composites Part A: Applied Science and Manufacturing. 2009;40(8):1090-110.
[38] Backman ME, Goldsmith W. The mechanics of penetration of projectiles into targets. International Journal of Engineering Science. 1978;16(1):1-99.
[39] Wang B, Xiong J, Wang X, Ma L, Zhang G-Q, Wu L-Z, et al. Energy absorption efficiency of carbon fiber reinforced polymer laminates under high velocity impact. Materials & Design. 2013;50:140-8.
[40] VanderKlok A, Stamm A, Dorer J, Hu E, Auvenshine M, Pereira JM, et al. An experimental investigation into the high velocity impact responses of S2-glass/SC15 epoxy composite panels with a gas gun. International Journal of Impact Engineering. 2018;111:244-54.

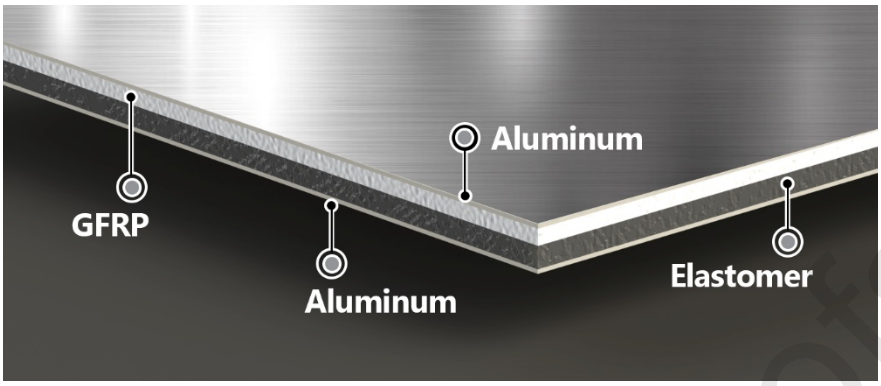

Fig. 1. Arrangement of various layers in the hybrid laminate

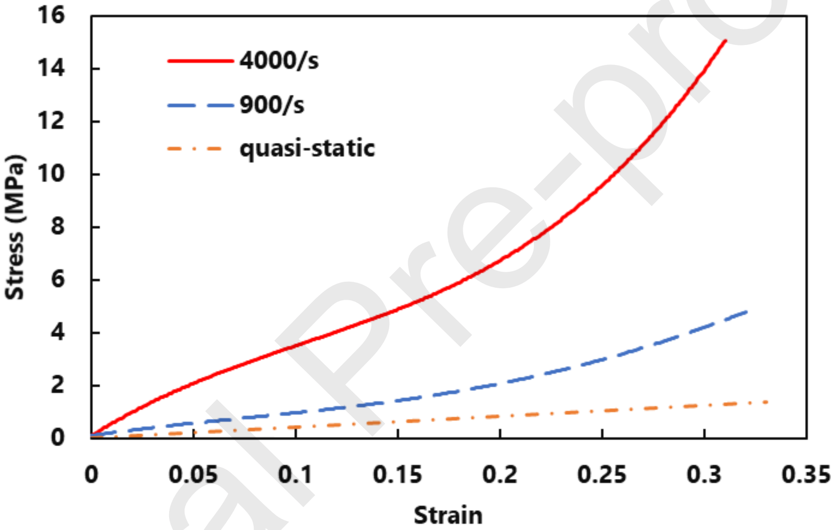

Fig. 2. Stress-strain curves for the elastomer at different strain rates

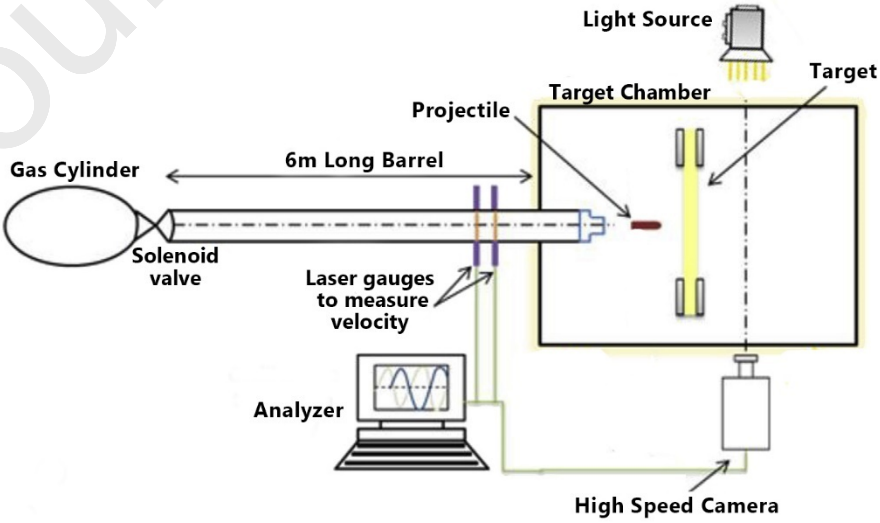

Fig. 3. Schematic of the gas gun apparatus

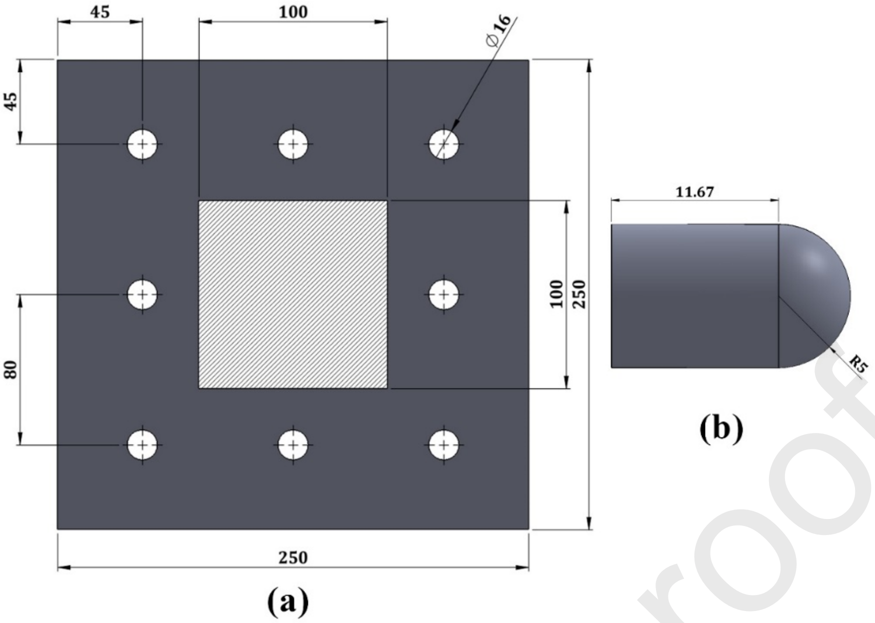

Fig. 4.(a) Schematic of fixture used for ballistic tests, (b) Technical drawing of projectile (dimensions in millimeter)

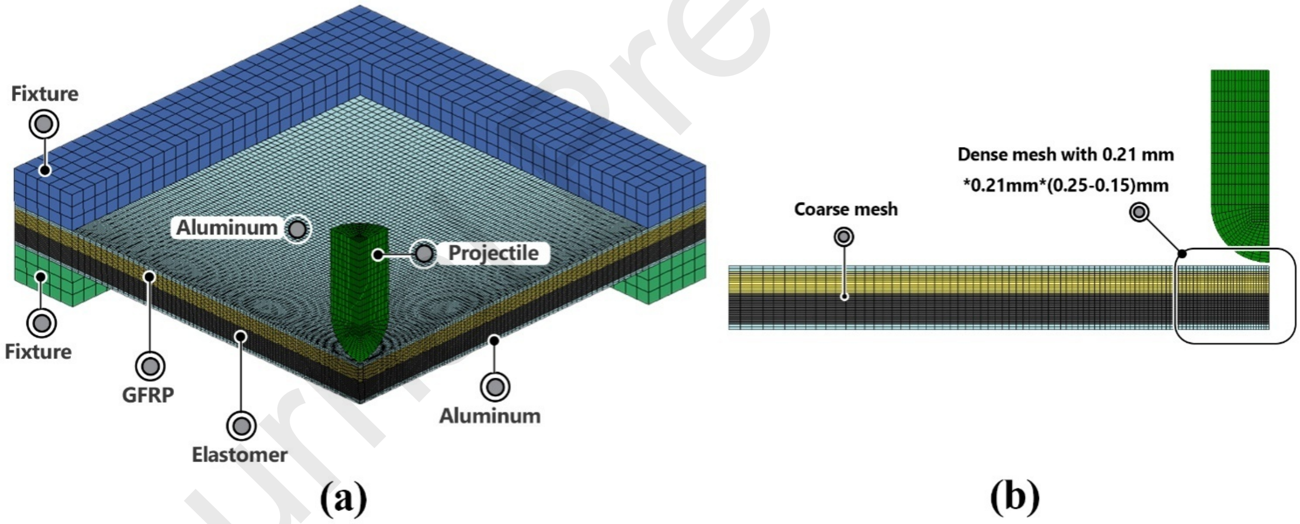

Fig. 5. (a) Isometric view and (b) Cross sectional view of the geometry modeling

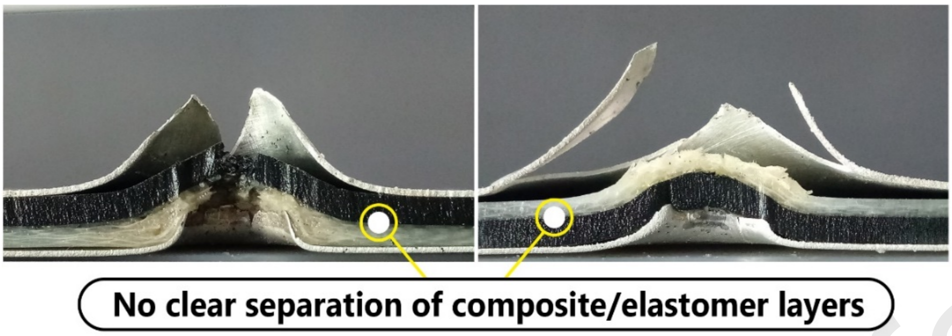

Fig. 6. No any observable delamination at the composite/elastomer interface

Fig. 7. Perforation mechanisms of the specimens in different impact velocities

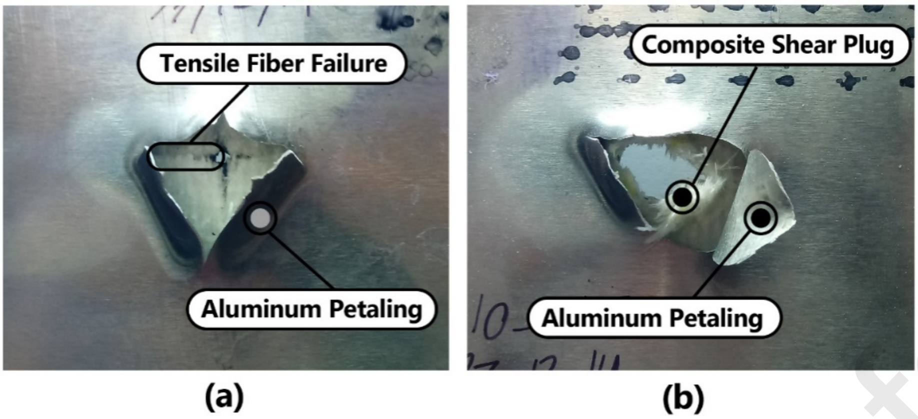

Fig. 8. Failure mechanisms in (a) EF-166 and (b) WE-166 specimens

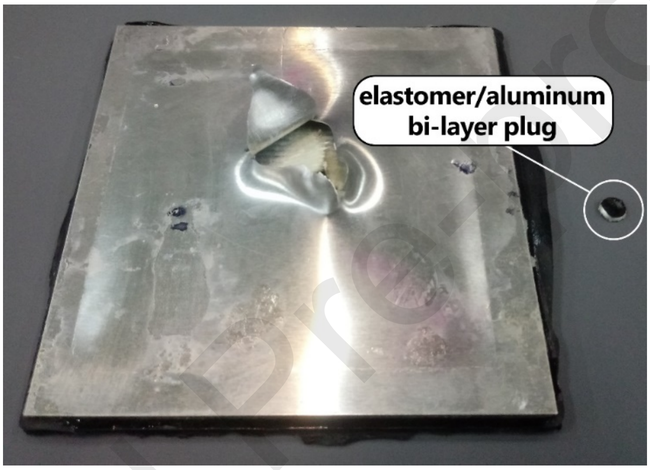

Fig. 9. Bi-layer plug ejected from EF-196 specimen

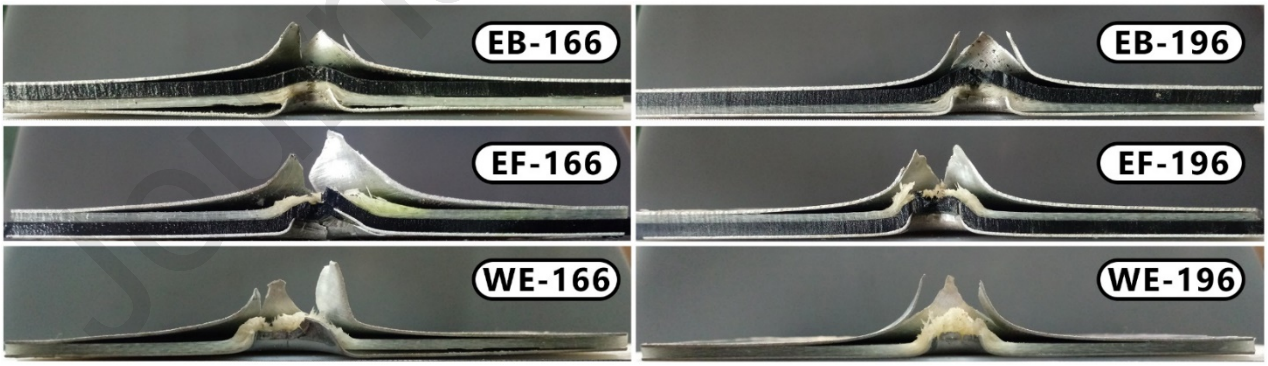

Fig. 10. Cross section of the specimens after perforation

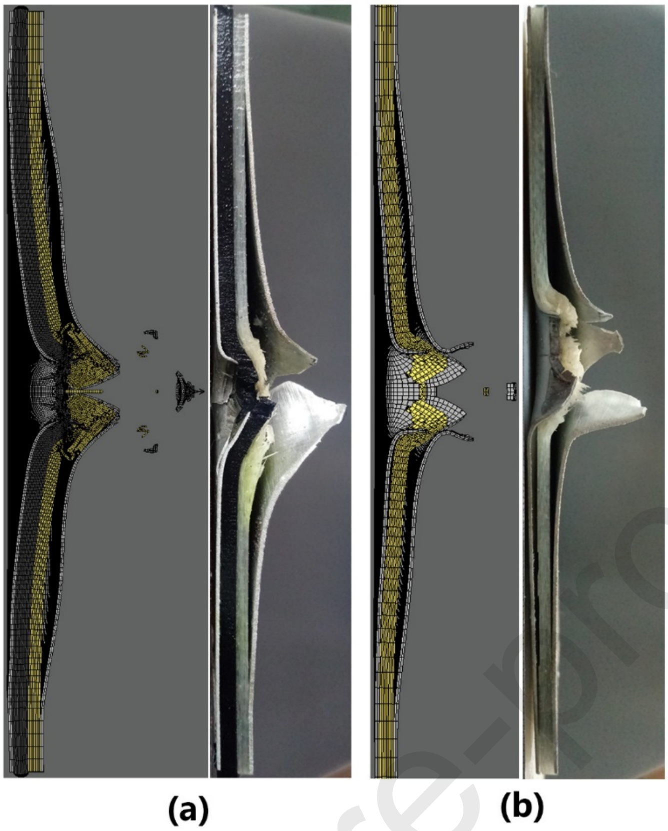

Fig. 11. Comparison of post-mortem configurations in EF-166 and WE-166 specimens during experimental and numericalassessments

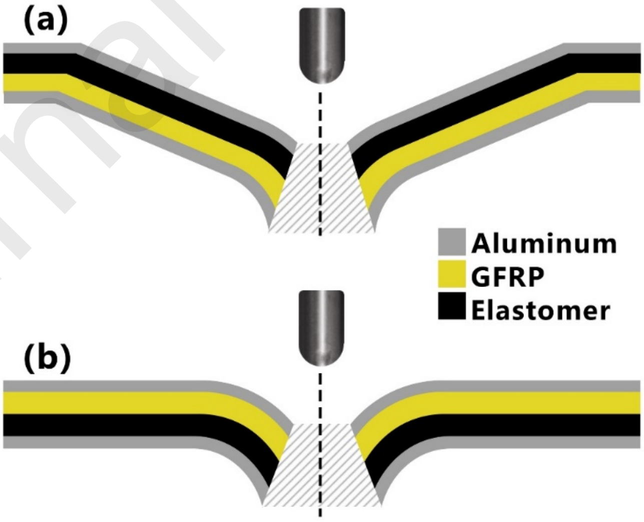

Fig. 12. Scheme of deformation profiles in (a) EF and (b) EB specimens

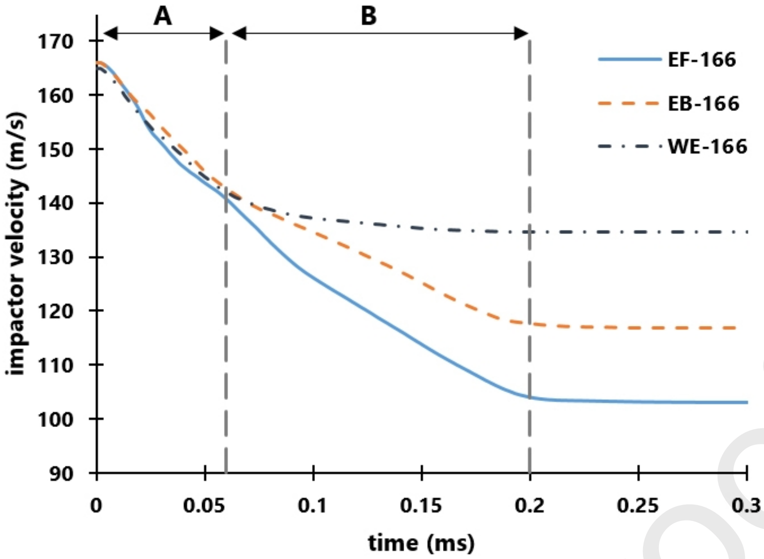

Fig. 13. Velocity time history of the different configurations at impact velocity of 166 m/s

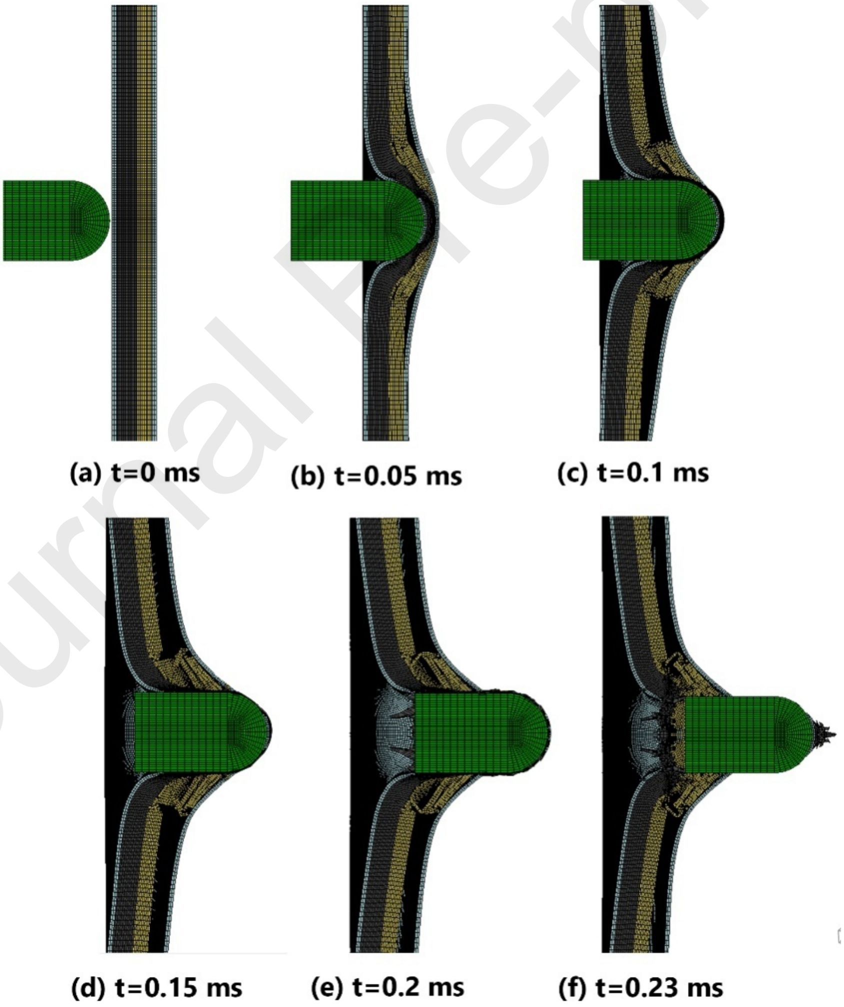
(a) t=0 ms (b) t=0.05 ms (c) t=0.1 ms

(d) t=0.15 ms (e) t=0.2 ms (f) t=0.23 ms

Fig. 14. Perforation time sequences of EF specimen at impact velocity of 166 m/s

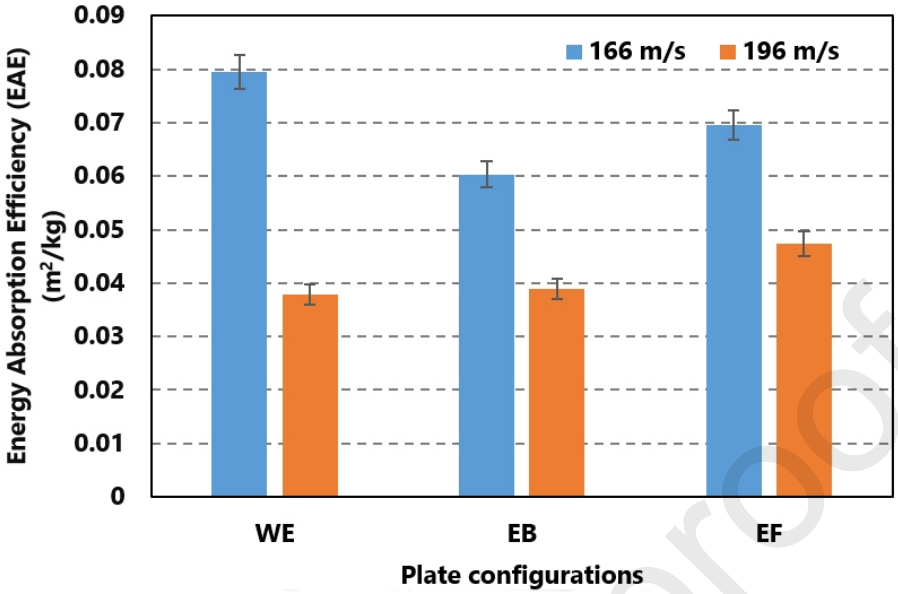

Fig. 15. Energy absorption efficiency of the specimens at different impact velocities

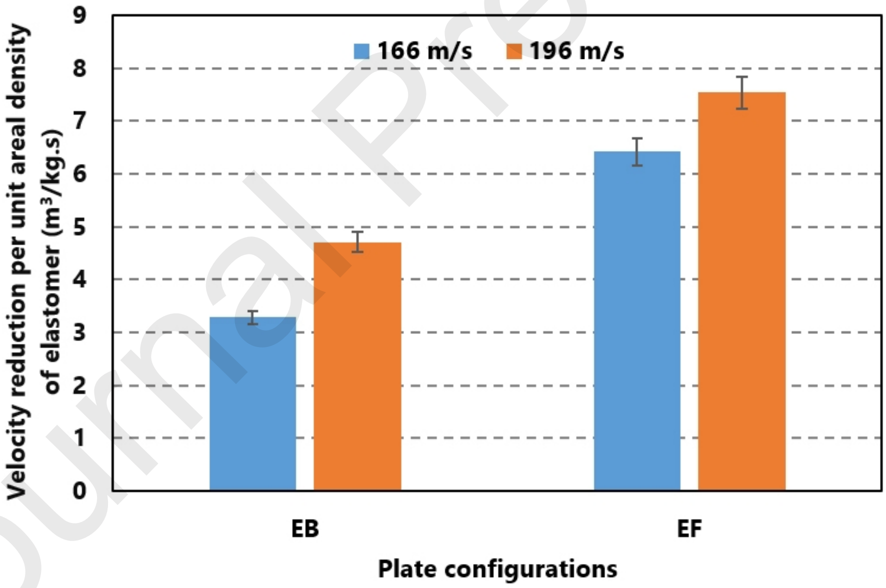

Fig. 16. Isolated elastomer performance at different impact velocities

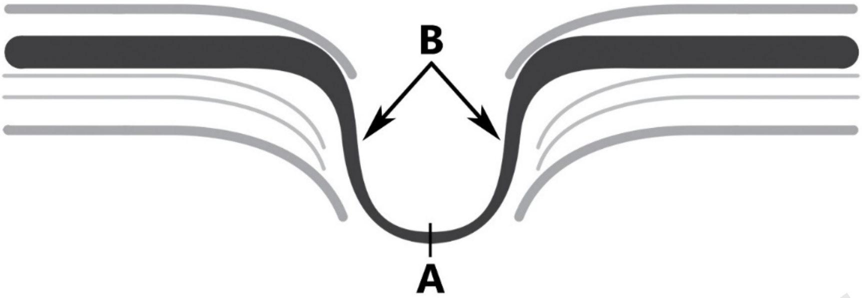

Fig. 17. Damage initiation point movement in elastomer at different velocities

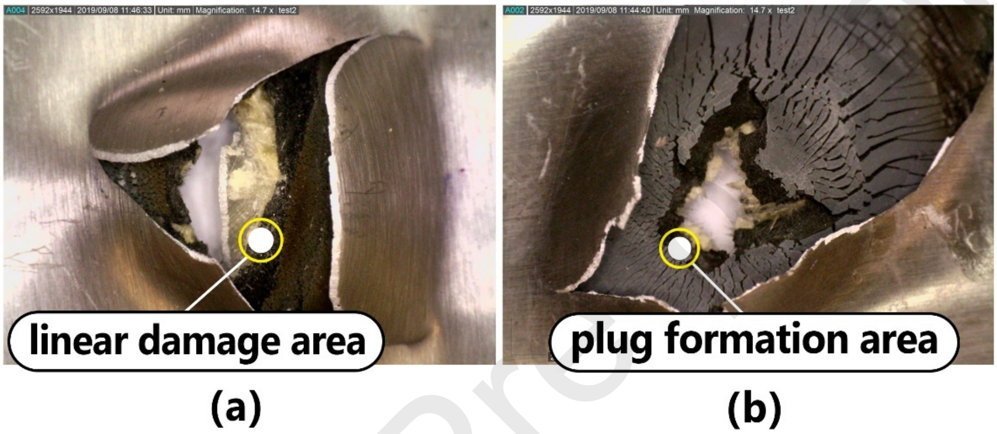

Fig. 18. Elastomer failure modes in (a) quasi-static indentation and (b) high velocity (196 m/s) perforation test

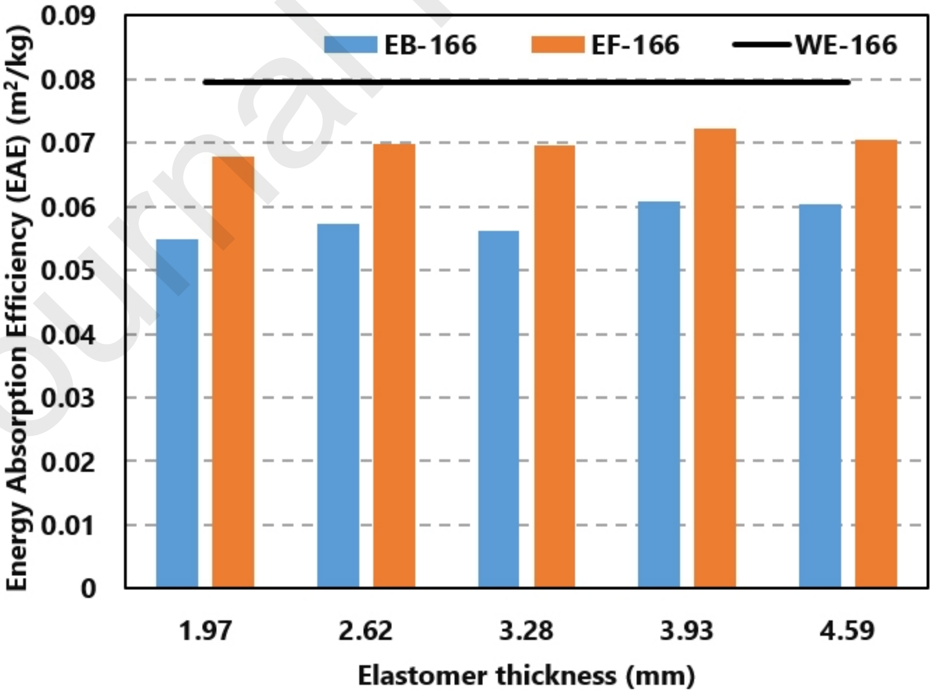

Fig. 19. Energy absorption efficiency at impact velocity of 166 m/s and different elastomer thicknesses

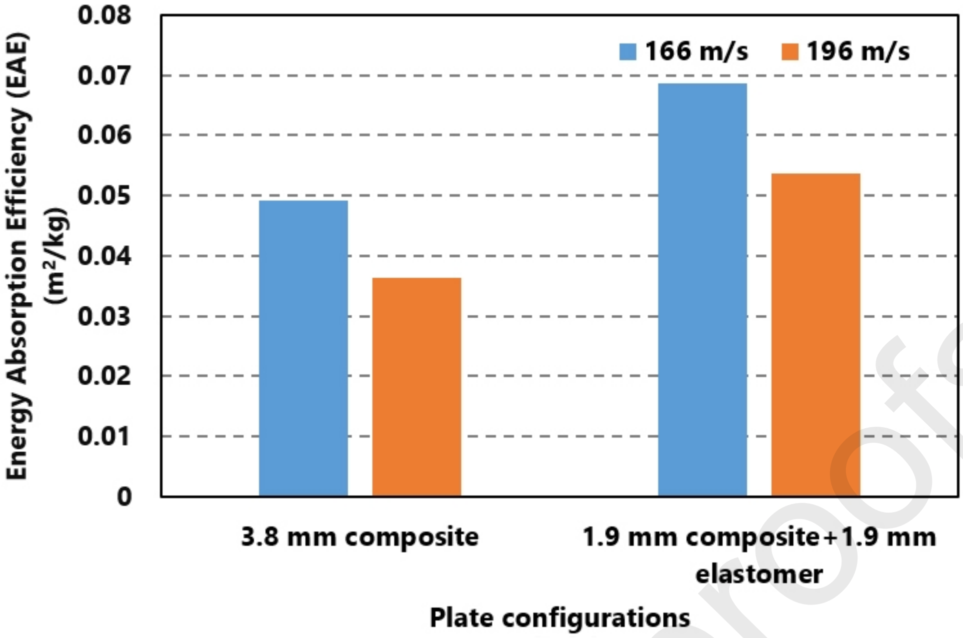

Fig. 20. Replacing half thickness of composite phase by an elastomeric layer

Table 1. Formulation of the compounded rubber

Ingredients	Loading (Phr)
NR	100
Carbon Black (N330)	60
Zink oxide	5
Calcium carbonate	30
Spindle oil	15
Sulfur	2
Coumarone resin	5
Stearic acid	1
Volcacit	0.7

Table 2. Mechanical properties of glass/epoxy composite

Property	Value
Density (kg/m^3)	1479.80
Fiber volume fraction (%)	40
Young's moduli, E_1, $E_{2,}$ E_3 (GPa)	19.93, 19.93, 4.76
Poisson's ratios, $\upsilon_{12}. \upsilon_{13}. \upsilon_{23}$	0.17, 0.414, 0.414
shear moduli, $G_{12,}$ $G_{13,}$ G_{23} (GPa)	1.49, 1.68, 1.68
tensile strengths, S_1, S_2 (MPa)	295.45, 295.45
compressive strengths, C_1, C_2 (MPa)	149.4, 149.4
shear strengths, $S_{12,}$ $S_{13,}$ S_{23} (MPa)	91.3, 50, 50

Table 3. Different configuration of tested specimens

Elastomer Backward (EB)	Elastomer Forward (EF)	Without Elastomer (WE)

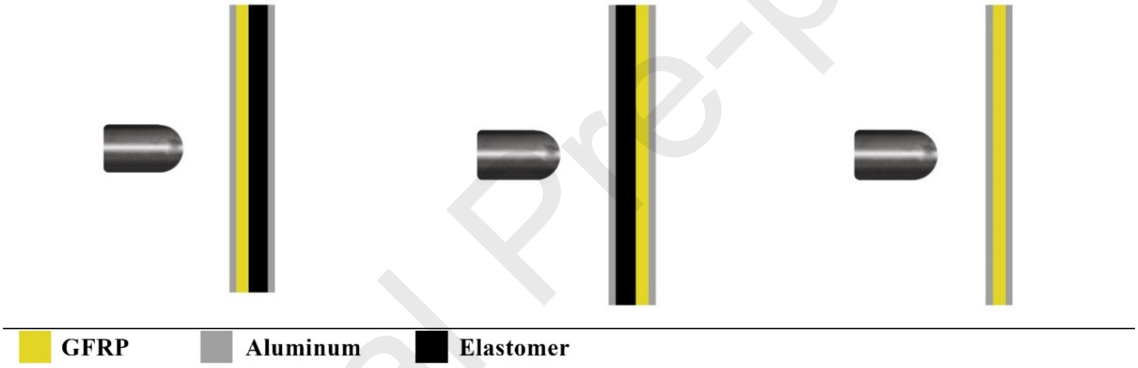

Table 4. Material constants used for aluminum 6061-T6 in numerical modeling [26]

Elastic constants		Plasticity constants		Failure constants	
E (GPa)	70.3	A (MPa)	270	D_1	-0.77
υ	0.28	B (MPa)	195	D_2	1.45
G (GPa)	26.4	n	0.3	D_3	-0.47
ρ(Kg/m^3)	2660	C	0.002	D_4	0.0
$\dot{\varepsilon}_0$ (1/s)	1	m	1.34	D_5	1.6

Table 5. GFRP property changes due to strain rate

Property	Percent of change	Reference
Tensile strengths	90, increase	[30]
Young’s modulus	10, increase	[31]
In-plane shear modulus	9, decrease	[32, 33]
In-plane shear strength	50, increase	[32]
Out-of-plane shear strength	90, increase	[34]
Compressive strength	78, increase	[35]

Table 6. Comprising numerical and experimental results

Configuration-impact velocity (m/s)	Experimental residual velocity (m/s)	Numerical residual velocity (m/s)
EB-166	113.5	116.8
EB-196	158.8	154.78
EF-166	103.2	102.9
EF-196	149.5	144.65
WE-166	124.3	134.7
WE-196	174.3	171.5